# Molecular Simulations as Tracking Tools for the Dynamics of Reactive Species: A Personal Retrospect

Rodrigo M. Cordeiro*

Reactive oxygen and nitrogen species (RONS) govern critical processes in biology and atmospheric chemistry, yet their fleeting dynamics often elude experimental tracking. Quantum chemistry is the go-to method for studying RONS, but fully classical molecular dynamics (MD) simulations, though unconventional for such transient species, offer unique insights into their interactions at complex interfaces. This self-reflective review chronicles a decade of our group's work developing the GROMOS-RONS force field, harnessing MD's computational efficiency to explore RONS in lipid bilayers, aquaporin channels, and water-air interfaces. These studies challenge the view of RONS as mere diffusible threats, revealing their selective enrichment and prolonged residence at critical interfacial regions. Simulations uncover nitro-oxidative pathways and transport mechanisms that shed light on unresolved experimental questions. Applications in signaling, therapy, and aerosol chemistry are highlighted, alongside challenges and future directions. By showcasing the GROMOS-RONS model's strengths for condensed-phase MD, we aim to inspire its broader application as a complementary tool to study RONS dynamics across diverse fields.

Graphical abstract
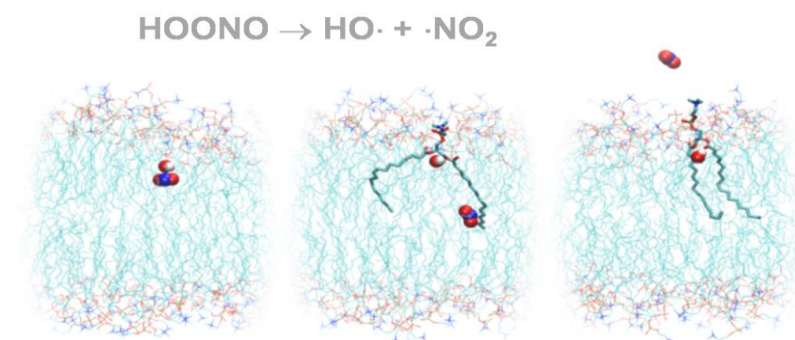
$$HOONO \rightarrow HO\cdot + \cdot NO_2$$

1. Introduction

Reactive oxygen and nitrogen species (RONS) encompass a class of small molecules, ions, and radicals characterized by their intrinsic reactivity and short lifetimes. These species exert profound influence across diverse scientific fields, including biochemistry and atmospheric chemistry. In living organisms, RONS drive essential redox signaling pathways that regulate cellular function [1,2]. Yet, when their production surpasses antioxidant defenses, oxidative stress emerges [3], potentially contributing to aging, carcinogenesis, and neurodegeneration [4-8]. This reactivity, however, also holds therapeutic promise. Techniques such as photodynamic therapy [9] and plasma medicine [10] harness artificially

Centro de Ciências Naturais e Humanas, Universidade Federal do ABC, Avenida dos Estados 5001, CEP 09210-580, Santo André (SP), Brazil. *Corresponding author. E-mail: **rodrigo.cordeiro@ufabc.edu.br**

generated RONS to induce localized cell death, demonstrating efficacy against neoplasms [11], bacterial infections, and tropical diseases [12]. Beyond biological systems, RONS play a pivotal role in atmospheric reactions and aerosol chemistry, among other domains [13].

In many of these domains, key RONS dynamics and reactions unfold at interfacial regions—whether the simple water-air boundary of an aerosol or the intricate, microheterogeneous environment of a cell membrane. For the latter, experimental studies to date have provided a broad qualitative perspective on RONS interactions and dynamics, using molecular probes to monitor their penetration into lipid bilayers [14-19]. However, these findings often carry significant uncertainty due to the mobility of probes, which prevents precise localization within the membrane [20]. This limitation highlights the need for deeper insights into RONS dynamics. To give one more example, in oxidative labeling experiments, protein topology is inferred from amino acid oxidation patterns triggered by RONS [21-24]. A clearer understanding of the specific interactions and pathways available to RONS could enhance the interpretation of oxidative labeling results.

Molecular dynamics (MD) simulations [25,26] stand out as a robust tool to address these issues. The simplicity and small size of RONS are attributes that render them ideal candidates for MD. Nonetheless, it is noteworthy that their exploration, especially in biomolecular simulations, emerged only relatively late [27-31]. This delay may stem from an initial reluctance, perhaps grounded in the belief that no method other than quantum chemistry could yield meaningful insights into RONS behavior. After all, a fully classical, non-reactive MD approach might seem, at first glance, an incomplete depiction, even at odds with the reactive essence of these species. Yet, what constitutes a short lifetime is a matter of perspective. To an experimentalist seeking to track RONS dynamics, a lifetime of 1 microsecond may appear fleeting, but for an MD theorist, it represents a vastly expansive timescale. Within the lifetime of RONS, many interesting events might occur—such as interactions with specific protein or membrane domains, partitioning across interfaces, or diffusion pathways. These events, in turn, may carry implications for reactivity. Even the highly reactive hydroxyl radical, known to react within 1 nanosecond [32], might conceivably engage in significant interactions and dynamical events during a typical MD run. As we will demonstrate through selected applications from our own work, while MD provides an admittedly partial view of RONS behavior in biological media, it nonetheless offers valuable clues that enhance the interpretation of experimental findings.

This review begins by presenting a molecular mechanical model for RONS simulations, which is the culmination of a decade of developments and refinements, primarily focused on biological applications [33]. What follows is a detailed exploration of its practical utility, probing RONS permeation and dynamics within phospholipid bilayers [30,34,35], their transport through protein channels [31], and their behavior at water-air interfaces [36]. In each instance, we emphasize specific insights from MD simulations that shed light on unresolved experimental questions. Through these examples, we aim to showcase the model's strengths as a tool for condensed-phase MD simulations and to inspire its broader application across diverse fields.

2. Development and Validation of a Molecular Mechanical Model for RONS

MD simulations of RONS require a force field that accurately captures their behavior in condensed-phase environments. In the biomolecular context, this means reproducing correct partitioning tendencies between aqueous media and less hydrophilic regions, such as phospholipid bilayers or protein interiors. Beyond partitioning, the force field must balance hydrogen bonds and ionic interactions to realistically depict specific RONS-biomolecule interactions. Over the past decade, we have developed molecular mechanical models for a comprehensive, though not exhaustive, array of RONS and related species [30, 31, 33, 34, 36, 37]. This set includes:

i) relatively stable species, such as hydrogen peroxide (H_2O_2) and molecular oxygen (O_2);

ii) short-lifetime oxyradicals, such as the hydoperoxyl ($HO_2\cdot$) and hydroxyl ($HO\cdot$) radicals;

iii) gases such as ozone (O_3) and various nitrogen oxides, including dinitrogen tetroxide (N_2O_4), nitrogen dioxide ($NO_2\cdot$), and nitric oxide ($NO\cdot$);

iv) peroxynitrous acid (HOONO), with its complex conformational landscape that includes *trans-perp*, *cis-perp*, and *cis-cis* conformers;

v) nitrogen oxyacids, namely nitric (HNO_3) and nitrous (HNO_2) acids—which, although not typically considered reactive species *per se*, may form as end-products of RONS reactions;

vi) nitrogen oxyanions, nitrate (NO_3^-) and nitrite (NO_2^-);

vii) anionic species, such as peroxynitrite ($ONOO^-$) and the superoxide radical anion ($O_2\cdot^-$).

The GROMOS force field [38,39] was selected as the foundation for these molecular mechanical models, owing to its empirical design and proven success in biomolecular simulations. Its parametrization protocol prioritizes the reproduction of reference solvation free energy data. Parametrization takes advantage from an extensive database of Henry's law constants for RONS [40]. Its tabulated values have been either directly measured or derived from related thermodynamic data, and they are continually refined as new measurements emerge. Robust phospholipid bilayer models, developed and validated within the GROMOS framework, are now widely adopted, further justifying the use of this force field [41,42]. The united-atom representation in GROMOS provides a computational efficiency advantage, particularly for the hydrocarbon tails of phospholipids, where non-polar hydrogens are merged with their respective carbon atoms into single interaction sites, reducing the cost of simulating non-polar regions. Earlier versions, such as 53A6 [38], were optimized for condensed-phase and biomolecular systems, while updates like 54A7 [39] improved protein structure descriptions and added post-translationally modified amino acids [43].

The parametrization of RONS followed a well-established route, leading to the so-called GROMOS-RONS force field [33]. Internal molecular structures—defined by bonds, angles, and dihedrals—were derived from electronic structure calculations or experimental data, such as spectroscopy and

crystallography. Bond stretching constants were not parametrized; instead, bond length constraints were applied to suppress high-frequency degrees of freedom, enabling larger simulation timesteps and enhancing computational efficiency without compromising the description of RONS dynamics in condensed-phase systems. Lennard-Jones (LJ) interactions and atom-centered partial charges were optimized to reproduce experimentally measured properties of RONS. For stable species like H_2O_2 and HNO_3, which form liquid phases under ambient conditions, standard GROMOS atom types failed to capture pure-liquid properties, such as density and heat of vaporization. The development of new atom types with tailored LJ parameters was required. For all electrically neutral RONS, partial charges were adjusted to reproduce reference hydration free energy data. Initial charge distributions, obtained from electronic structure calculations, served as starting points for solvation free energy calculations via thermodynamic integration [26]. These often underestimated hydration free energies, requiring iterative scaling to account for solvent-induced polarization until agreement with experimental benchmarks was achieved [40, 44].

For gaseous species, where solvation data in both aqueous and hydrocarbon media are available [45-50],

parametrization targeted accurate partitioning across hydrophilic and hydrophobic environments. This dual requirement posed a challenge, particularly for small molecules like O_2. In a GROMOS-type O_2 model, symmetry dictates zero partial charges on oxygen atoms, leaving LJ terms as the sole adjustable parameters (unless, of course, virtual interaction sites are introduced to capture effects like quadrupole moments or electron lone pairs). Without virtual sites, balanced solvation in water and hydrocarbons relied on developing new atom types with tailored LJ parameters.

As shown in Fig. 1, this approach yielded solvation free energies in close agreement with reference data in the case of electrically neutral RONS. For ionic RONS, the focus shifted to accurately reproducing hydration structures and experimentally observed ion-pairing tendencies. For example, in $NaNO_3$ solutions up to 4 mol/L—a concentration range relevant to biomolecular and atmospheric chemistry— simulations achieved good agreement with experimental ion-pairing data [51], as shown in Fig. 1. This balance of ionic interactions highlights the model's reliability in biologically and environmentally relevant contexts. The development and validation of this GROMOS-RONS force field are thoroughly documented, offering a transparent framework that facilitates extension to additional species.
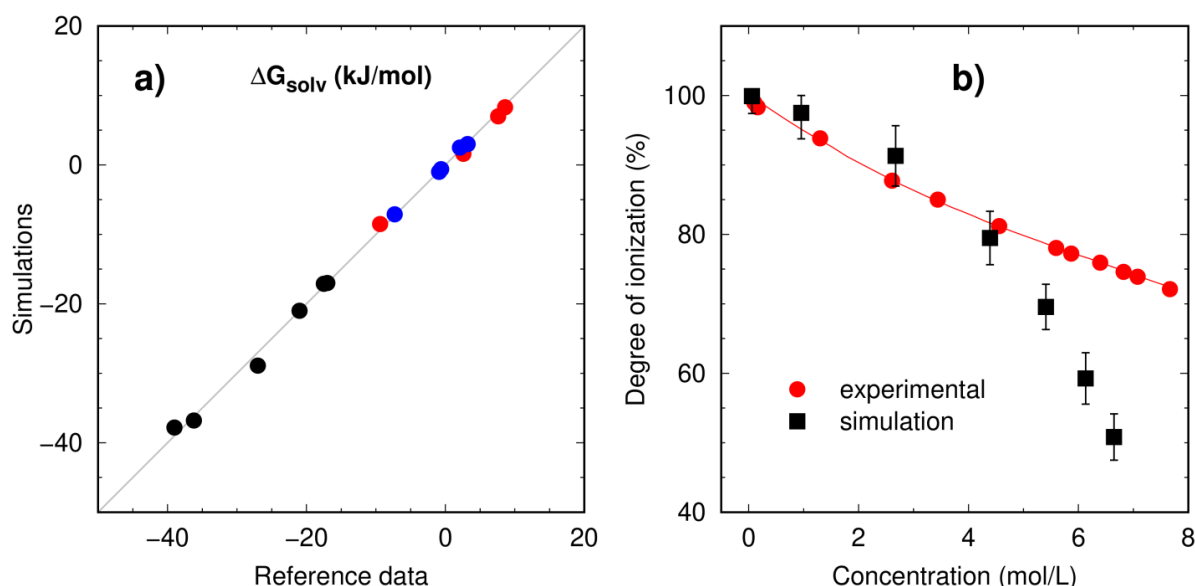
Fig. 1. (a) Comparison between solvation free energies of RONS from simulations and reference experimental/thermodynamic data [40,44-50]. Data include hydration of hydrophilic, electrically neutral species (black), hydration of gaseous species (red) and solvation of gaseous species in hydrocarbons (blue). (b) Concentration-dependent ion pairing in $NaNO_3$ aqueous solutions from simulations and experiments [51]. Data replotted from ref. [33].

## 3. Oxygen Enrichment in Phospholipid Bilayers: The Membrane Lens Effect

The so-called "Membrane Lens Effect" describes how phospholipid bilayers concentrate small, hydrophobic molecules like O_2 within their interior, enhancing local reactivity or availability [52]. Bilayers are microheterogeneous environments with position-dependent properties [53] such as dielectric constant, free volume, and molecular ordering, resulting in non-uniform distributions for small permeants like O_2. This complexity distinguishes membranes from model solvents, where molecular packing and orientation are simply isotropic. Consequently, solubility data on model solvents are

not directly transferable to membranes.

The GROMOS-RONS force field been successfully employed in MD simulations of O_2 distribution within dipalmitoylphosphatidylcholine (DPPC) bilayers across a broad temperature range, spanning both gel and fluid phases [35]. Fig. 2 shows that O_2 distribution strongly depends on the bilayer phase. In fluid-phase DPPC, O_2 concentration at the headgroup region dipped slightly below bulk water levels, then rose monotonically toward the bilayer center. In gel-phase DPPC, the profile shifted dramatically: O_2 dropped from the aqueous phase to the headgroups and remained nearly depleted along the phospholipid tail region. O_2 accumulation occurred only near the bilayer center, where the free volume between leaflets allowed a concentration spike. Averaging of

the local O_2 concentrations across the bilayers yielded water-to-membrane partition coefficients comparable to experimental data [54,55]. Simulations suggest that the bilayer phase state exerts a stronger influence than temperature alone. Across the main transition temperature (T_m), the partition coefficient tripled from the gel to the fluid phase, reflecting O_2's preference for disordered lipid regions.

While these results aligned reasonably well with experimental findings, the effect of the gel-to-fluid transition appeared sharper in simulations than in experiments. This discrepancy likely stems from the small, uniform-phase systems simulated, whereas real membranes feature coexisting domains near T_m, which are responsible for smoothing the shift.
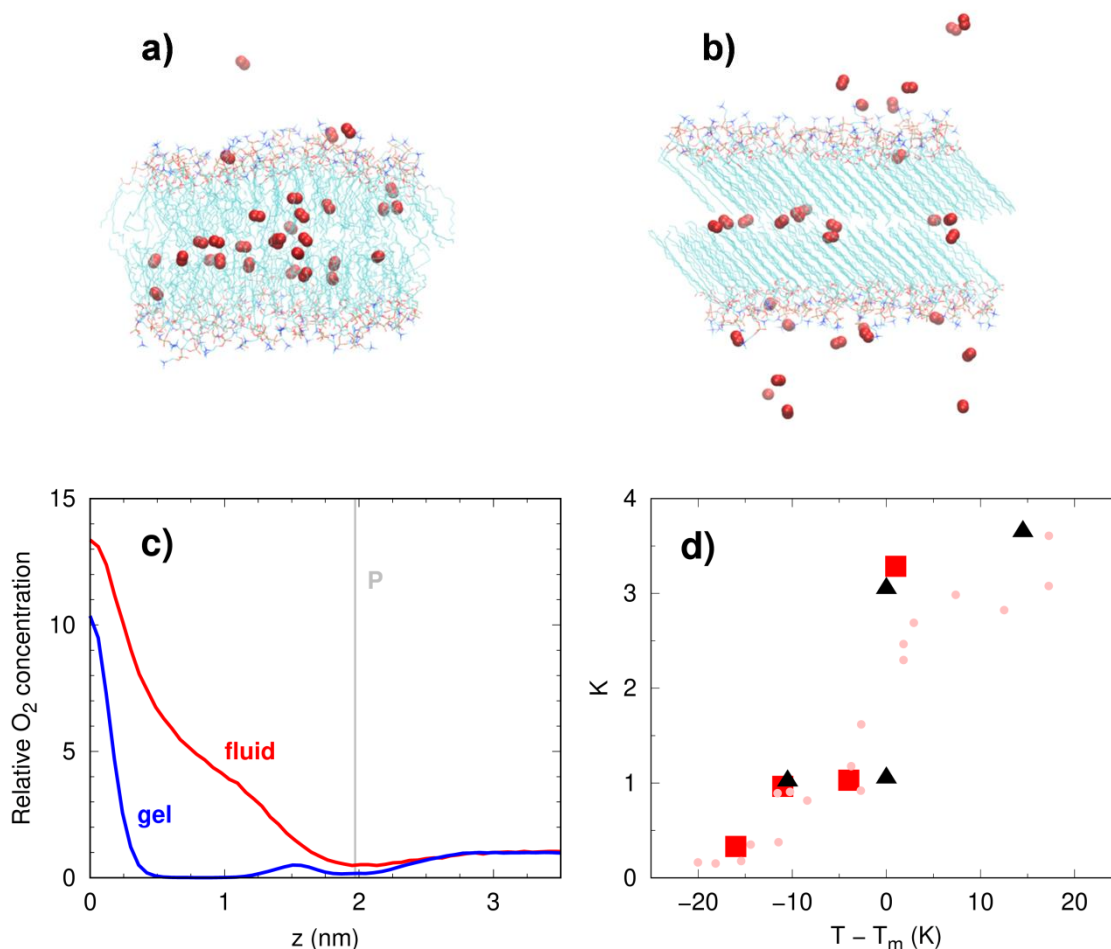
Fig. 2. Simulation snapshots showing O_2 enrichment and distribution in DPPC bilayers at the (a) fluid and (b) gel states. Water molecules were omitted for clarity. (c) Local O_2 concentration (relative to the bulk aqueous phase) as function of the distance z to the bilayer center. The vertical line marks the average position of the headgroup phosphate groups (P) at the membrane-water interface. (d) Water-to-membrane partition constant K of O_2 as function of temperature. Simulation (black triangles) and experimental [54] (red squares) data are shown for DPPC, along with experimental data for dimyristoylphosphatidylcholine [55] (pink circles). Data replotted from ref. [35].

The ability of the GROMOS-RONS force field to describe O_2 distribution across different membrane phases holds biochemical significance. Membranes are not always in the fluid phase; for instance, experimental evidence supports a gel-phase model of the mammalian skin barrier [56]. Moreover, biological membranes often contain phase-separated domains that vary considerably in composition, fluidity, and lipid ordering. Cholesterol-enriched lipid rafts [57] are the most emblematic examples, but evidence also exists for sterol-independent, gel-like rafts in the plasma membranes of living cells [58,59]. This multitude of lipid states reinforces the need for an accurate understanding of how oxygen distribution varies with temperature and membrane phase. Besides that, respiration, lipid peroxidation, and photosensitized singlet oxygen ($^1O_2$) generation in photodynamic therapy are examples of processes that depend on local O_2 availability. Indeed, it has been proposed

that photosensitizers that are able to penetrate deeper into the O_2-rich membrane interior lead to enhanced $^1O_2$ production [60], a trend linked to the Membrane Lens Effect [61,62]. These applications clearly benefit from MD models that balance aqueous and hydrophobic solvation. By capturing these features, the MD simulations based on the GROMOS-RONS force field not only explain reactivity amplification but also provide a tool to probe membrane biophysics where experimental resolution may be limited.

4. Oxyradical Accessibility to Phospholipid Membrane Oxidation Sites

The effects of RONS in the organism are largely influenced by their interactions with phospholipid membranes. Reactions are compartmentalized according to the membrane-crossing

ability of RONS, which varies among different species [63]. The Membrane Lens Effect may play out not necessarily as accumulation in the membrane interior, but rather as a tendency for binding, enrichment, and prolonged residence times at the membrane surface. Thus, certain reactions may be favored at the membrane-water interface. MD simulations based on the GROMOS-RONS force field have offered important insights into some of these aspects [30]. As depicted in Fig. 3, simulations revealed that even hydrophilic species, such as $HO_2\cdot$ and $HO\cdot$ radicals, may reside at the membrane-water interface and penetrate deep into the lipid headgroup region. Although the membrane poses a permeation barrier to these radicals, their affinity for the headgroups—coupled with membrane fluidity and disorder—enables access to peroxidation sites without the need to fully traverse the membrane. Indeed, Fig. 3 highlights a significant overlap between oxyradical distributions and the double-bond region of phospholipid tails, a key peroxidation target. This effect also suggests that radical scavengers and antioxidants, whose efficacy depends on their location (i.e. membrane interior vs. interface), must align with RONS distributions to neutralize oxidative threats effectively.

The role of $HO_2\cdot$ in lipid peroxidation has often been overlooked, as it predominantly exists as its conjugate base, $O_2\cdot^-$, at physiological pH [64]. Yet, simulations showed $HO_2\cdot$ concentrating in the headgroup region at levels significantly higher than in bulk water (c.f. Fig. 3). In contrast, the ionic $O_2\cdot^-$ is expected to remain largely excluded from the headgroup region due to its strong hydrophilicity. The $HO_2\cdot$ enrichment suggests a local pK_a shift near the membrane, favoring its protonated form over $O_2\cdot^-$. Simulations support experimental data sugesting that the importance of $O_2\cdot^-$ for lipid peroxidation stems from its ability to form $HO_2\cdot$ [65-68]. Even at physiological pH, $HO_2\cdot$ may thus play a significant role in lipid peroxidation and radical scavenging by membrane-bound antioxidants.
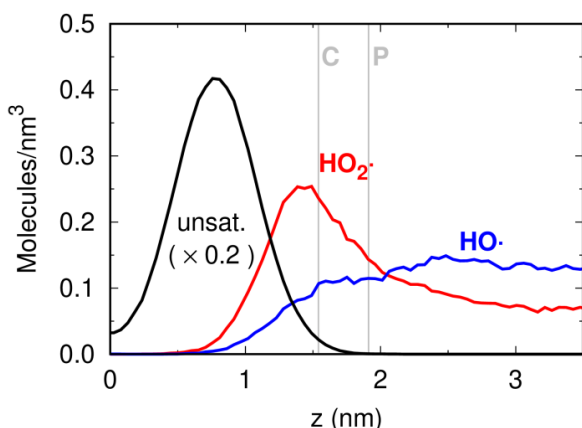
Fig. 3. Distribution of oxyradicals in a 1-palmitoyl-2-oleoyl-sn-glycero-3-phosphocholine (POPC) bilayer. Local concentrations of oxyradicals are expressed as function of the distance *z* to the bilayer center, along with the scaled distribution of unsaturations along the phospholipid tails. Vertical lines indicate the average positions of carbonyl ester (C) and phosphate (P) groups at the membrane-water interface. Simulations followed the protocol outlined in ref. [30], with updated $HO_2\cdot$ parameters [31,33].

Although classical MD models cannot explicitly describe chemical reactions, they effectively capture subtle interfacial effects that influence reactivity. Specific RONS-membrane interations may affect the way in which different lipid types

and membrane compositions respond to oxidative stress. Independent simulations have suggested that RONS-induced lipid oxidation enhances the membrane permeability to RONS, leading to a feedback loop that amplifies oxidative stress [69]. Conversely, the presence of cholesterol in the membrane has been found to hamper RONS permeation [70].

The intricate interplay between RONS and phospholipid membranes underscores a delicate balance between oxidative damage and cellular resilience. MD simulations, empowered by force fields like GROMOS-RONS, have illuminated the nuanced dynamics at the membrane-water interface, revealing how species like $HO_2\cdot$ and $HO\cdot$ exploit membrane fluidity and headgroup affinity to access peroxidation sites. These insights challenge traditional views of RONS as mere diffusible threats, highlighting instead their selective enrichment and prolonged residence at critical membrane regions. The unexpected prominence of $HO_2\cdot$ at the membrane-water interface further emphasizes the need to reconsider its role in lipid peroxidation alongside its conjugate base, $O_2\cdot^-$. While these findings mark significant strides, the journey is far from complete. Systematic investigations into how membrane composition, lipid diversity, and structural variations modulate RONS permeation and reactivity are essential to unravel the full scope of oxidative stress mechanisms. Such studies promise not only to deepen our understanding of membrane dynamics but also to guide the development of targeted antioxidant strategies, paving the way for innovative therapeutic interventions against oxidative stress-related pathologies.

5. Peroxynitrous Acid at Membrane Interfaces: Insights into Localized Reactivity

Peroxynitrite, $ONOO^-$, is a potent and relatively stable oxidant that forms *in vivo* through the rapid reaction between $NO\cdot$ and $O_2\cdot^-$ radicals [71]. At physiological pH, it coexists in equilibrium with significant amounts of peroxynitrous acid, HOONO [44], which undergoes O—O bond homolysis to produce $NO_2\cdot$ and the highly reactive $HO\cdot$ radical [8]. This formation outpaces the Fenton-type production of $HO\cdot$ from H_2O_2 by a factor of at least a million [72,73]. Unlike $HO\cdot$, which reacts almost immediately near its origin, $ONOO^-/HOONO$ can travel micrometer distances, triggering nitro-oxidation processes far from their formation site [74,75]. While $ONOO^-$ requires anion channels to cross cell membranes, ONOOH readily diffuses through them passively [76]. Experimental evidence suggests that ONOOH homolysis may be favored in the hydrophobic membrane interior, as compared to aqueous environment [17-19]. However, the underlying mechanisms remain unclear.

As shown in Fig. 4, HOONO presents a complex conformational landscape, shaped by the interplay of its O—N—O—O and N—O—O—H dihedral angles. For simplicity, dihedral angles near 0°, 60°, 90°, and 180° are denominated as *cis*, *gauche*, *perp*, and *trans*, respectively. In the gas phase, the *cis-cis* conformer corresponds to the global energy minimum, due to its planar ring-like structure that preserves an intramolecular hydrogen bond [77]. Rotation about the O—O bond axis leads through a modest barrier to the *cis-perp* local minimum. Although the *cis-perp* conformer has higher energy than *cis-cis* in the gas phase, the situation changes in the aqueous phase. The *cis-perp* conformer gains importance in solution due to competition from water molecules for

hydrogen bonds with HOONO. Rotation about the N—O bond axis yields the *trans-perp* conformer. However, this transition is hampered by a steep energy barrier that limits isomerization at physiological temperatures. It is challenging to devise a unique classical model that accounts for the structure of all

HOONO conformers. Electronic structure calculations have revealed a moderate coupling between rotameric states and the N—O bond length [77-79]. Yet, despite these limitations, the GROMOS-RONS force field delivers an accurate description of HOONO conformational energies (Fig. 4).
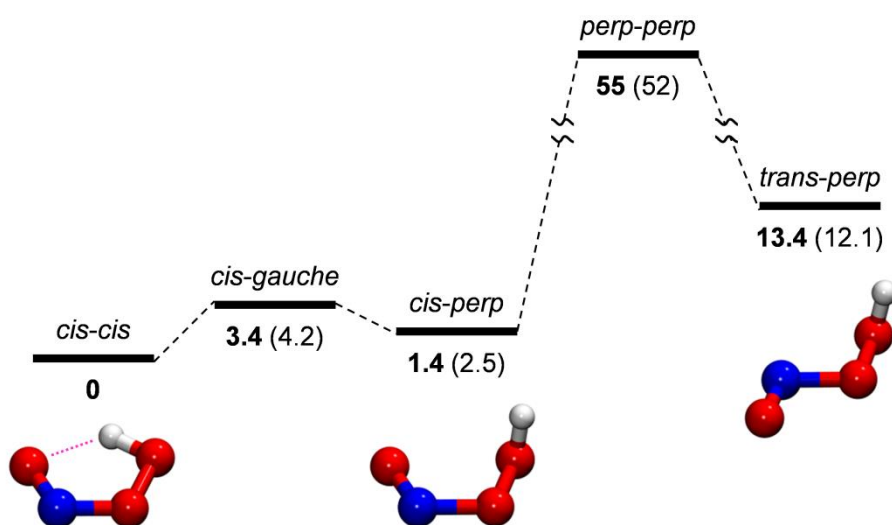
Fig. 4. Schematic representation of the conformational energies of gas-phase HOONO. Energies (in kJ/mol) obtained from the GROMOS-RONS classical force field (bold) are compared to results from electronic structure calculations [77] (within brackets).

MD simulations based on GROMOS-RONS have confirmed that HOONO behaves like a small amphiphile. Its terminal —OH group, strongly hydrophilic, forms hydrogen bonds with water, while the hydrophobic —ONO fragment induces a solvent cage. This dual nature sets the stage for its interactions with phospholipid membranes. In fact, MD simulations revealed a strong tendency of HOONO to bind and accumulate at the headgroup region, driven in part by stable hydrogen bonds with phospholipid carbonyl ester groups, hydration waters, and likely aided by its surfactant-like structure [34]. This binding affinity, combined with membrane fluidity and disorder, positions HOONO to access oxidizable sites along phospholipid hydrocarbon chains.

Classical MD models excel at capturing partitioning and permeation phenomena, but their inability to explicitly account for electronic degrees of freedom precludes direct simulation of chemical reactions like HOONO homolysis. Studying homolysis directly would require computationally demanding quantum mechanical/molecular mechanical methods or reactive force fields. Instead, a simplified yet insightful approach has been proposed [34], solely based on classical MD with the GROMOS-RONS force field. After equilibration of a phospholipid membrane in the presence of HOONO, the O—O bonds were cleaved by releasing their constraints, effectively transforming HOONO molecules into HO·/NO$_2$· radical pairs. The initial HOONO coordinates served as starting points for the trajectories of these radicals post-homolysis. As shown in Fig. 5, the radical pairs separated rapidly, within less than 1 ns. Most NO$_2$· radicals migrated to the membrane interior, but they eventually made excursions to the aqueous phase. Since MD simulations were based on a closed system, these escapees eventually re-entered the membrane, but in an open system, most would likely diffuse away into the bulk water. For HO·, about one-third of the radicals escaped to the aqueous phase within 1 ns. Surprisingly, however, a significant fraction lingered at the headgroup region, stabilized by hydrogen bonds with carbonyl

ester groups and hydration waters, with residence times extending to ~50 ns. This persistence was unexpected, given prior data suggesting no particularly strong HO· affinity for the membrane surface (Fig. 3). It has been proposed that HOONO generates HO· radicals in positions less accessible to exogenously introduced HO· from the aqueous phase. In these positions, HO· radicals from HOONO homolysis become trapped in metastable configurations at the headgroups, likely driven by local hydrogen-bonding interactions. While many HO· radicals dissipate into the aqueous phase post-homolysis, those that remain may enhance nitro-oxidation reactions within the membrane interior. This behavior offers a potential explanation for the heightened efficiency of HOONO-induced reactions in membrane environments [17-19].

The GROMOS-RONS force field has proven instrumental in elucidating the dynamics of HOONO at phospholipid membrane interfaces, revealing its amphiphilic binding and the post-homolysis trajectories of HO· and NO$_2$· radicals. Classical MD simulations, despite their inability to model chemical reactions directly, offer critical insights into localized nitro-oxidation processes, particularly the unexpected persistence of HO· at the headgroup region. By capturing these subtle interfacial effects, the model not only clarifies the mechanisms driving HOONO enhanced reactivity in membranes but also demonstrates its versatility for broader RONS studies.

6. Aquaporins as Transmembrane RONS Transporters

Aquaporins are transmembrane proteins that orchestrate the passive flow of water across phospholipid bilayers [80,81]. Structural studies have unraveled their basic architecture: alpha-helix bundles form a narrow pore lined with hydrophilic side chains, guiding water into a single-file procession [82-84]. Selectivity hinges on two critical checkpoints: the Asn-Pro-Ala

(NPA) motifs at the pore's center block protons and ions, while the aromatic/arginine (ar/R) constriction near the extracellular exit fine-tunes passage [85-93]. Yet, aquaporins are more than water conduits. Growing evidence suggests they transport H_2O_2 [94-96] and possibly other RONS, reshaping our understanding of their biological significance. In plants and algae, RONS exposure can reversibly throttle aquaporin conductivity, suggesting an oxidative gating mechanism [97-99]. This interplay positions aquaporins as both regulators and responders in oxidative stress scenarios.
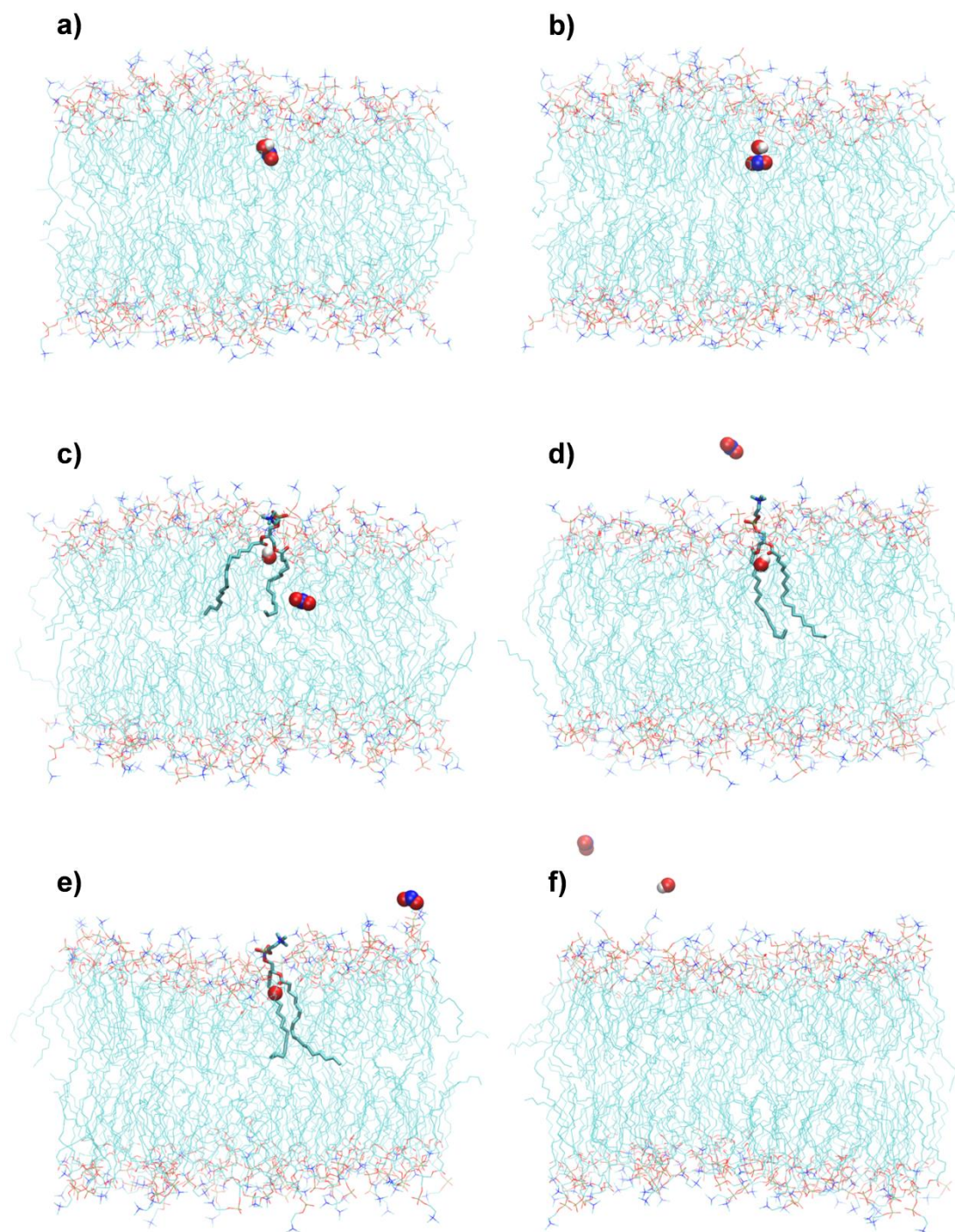
Fig. 5. Sequence of events after homolysis of a selected membrane-bound HOONO molecule. (a) Equilibrated HOONO molecule at its preferred position in the membrane headgroups region. (b) HO·/NO$_2$· radical pair configuration formed after splitting of the O—O bond, followed by energy minimization and thermalization. (c) Rapid separation of the radical pair, in which NO$_2$· populates the membrane interior, while HO· establishes a hydrogen bond with the highlighted phospholipid (*t* = 1 ns). (d) The NO$_2$· radical is lost to the aqueous phase, while HO· remains bonded to the headgroup region (*t* = 22,2 ns). (e) In this particular case, HO· bonding persists for longer durations (*t* = 46 ns). (f) HO· is eventually lost to the aqueous phase (*t* = 47,8 ns).

The GROMOS-RONS force field has enabled a systematic study of RONS transport by aquaporins [31]. MD simulation results support the notion that aquaporins don't just manage water—they channel H_2O_2 with remarkable efficiency. Fig. 6

shows that the energy barrier for H_2O_2 permeation through mammalian AQP1 is comparable to that for water and substantially lower than that through a bare POPC bilayer. Comparable findings were observed for plant PIP2;1 (data not shown). Early investigations into H_2O_2 permeation through aquaporins produced varied results. For instance, expressing certain plant aquaporins in yeast reduced cell growth and survival under H_2O_2 exposure, suggesting a role in H_2O_2 transport, whereas human AQP1 expression had no effect on yeast viability [94]. Later studies proposed that this apparent lack of H_2O_2 transport might stem from low expression levels

rather than an intrinsic limitation [100]. However, recent work by Orrico *et al.* demonstrated that H_2O_2 permeability across human erythrocyte membranes is independent of AQP1 or AQP3, with simple diffusion through the lipid fraction being the dominant mechanism [101,102]. These findings suggest that H_2O_2 transport mechanisms might be highly context-dependent, varying by cell type and membrane composition. MD simulations remain valuable for probing these differences, but caution is warranted when extrapolating to diverse biological systems, and further studies are needed to clarify aquaporin roles across different contexts.
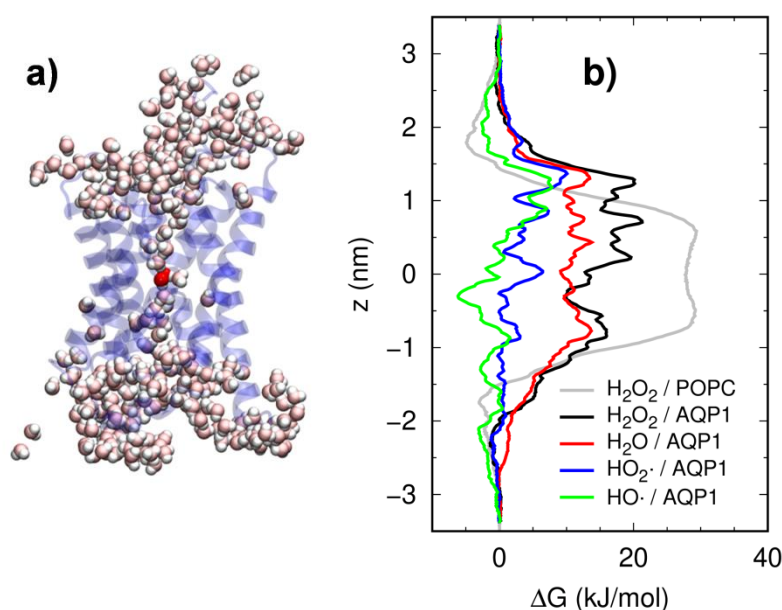
Fig. 6. (a) Simulation snapshot showing H_2O_2 permeation through human AQP1 aquaporin monomer. For clarity, water molecules inside the pore are represented in faded colors. (b) Permeation free energy profiles of H_2O_2, water and oxyradicals accros AQP1 and POPC membranes. Data replotted from refs. [30,31].

MD simulations support the involvement of aquaporins in the transport of other RONS [31,103-105]. Free energy profiles (Fig. 6) for $HO_2\cdot$ and $HO\cdot$ uncover even lower permeation barriers at the pore region compared to water or H_2O_2. This finding suggests aquaporins may play a broader role in RONS transport, carrying implications for signaling and therapeutic applications. For example, aquaporin overexpression in cancer cells might partly account for their heightened sensitivity to RONS-based therapies [106]. Even highly reactive $HO\cdot$ radicals, diffusing from solution, could plausibly breach the pore's vestibular region and oxidize exposed residues, though whether they are able to fully traverse the pore remains contentious. Oxidative labeling experiments have demonstrated HO-induced oxidation of inner pore residues [107,108]. Yet, it remains unclear whether these $HO\cdot$ radicals, which are produced via H_2O_2 photolysis, arise locally from H_2O_2 already within the pore or form near the entrance and penetrate inside. The shallow energy barriers revealed by MD simulations lend weight to the latter scenario. By contrast, $HO_2\cdot$ might fare better in full permeation, potentially serving as a biologically relevant shuttle for $O_2\cdot^-$ through the channel.

7. Probing Aerosol Chemistry through Acid-Base and Ion-Pairing Equilibria at Interfaces

While previous sections of this review explored RONS in biological systems like membranes and channels, the GROMOS-RONS force field also illuminates their behavior—and that of related species—in atmospheric chemistry. At the water-air interface, molecules may exhibit distinct enrichment or depletion patterns that influence aerosol chemistry. In fact, prior MD simulations have shown that small oxyradicals tend to accumulate at water surfaces [109-111]. MD simulations resolve solute distributions along this interface with fine spatial detail, but their reliability strongly depends on the force field's quality. In this context, the GROMOS-RONS force field emerges as an useful asset, given its well-balanced and validated performance in describing solvation and ion-pairing interactions. To exemplify its applicability, consider the following effect. Spectroscopic measurements [112] and *ab initio* calculations [113-116] show that HNO_3, is stabilized at the water-air interface in its protonated form, behaving as a weaker acid there. Can the GROMOS-RONS force field capture this effect, at least qualitatively?

Classical, non-reactive force fields like GROMOS-RONS cannot simulate protonation or deprotonation events, as these processes require explicit consideration of electronic degrees of freedom. Nevertheless, they are powerful tools for exploring how interfaces accomodate different species. Specifically, an interface-induced pK_a decrease for nitric acid should manifest as interfacial enrichment of HNO_3 and depletion of NO_3^-. This behavior, conceptualized by the thermodynamic cycle in Fig. 7a, is well within the capabilities

of the GROMOS-RONS force field. Fig. 7b shows the spatial distributions of HNO_3 and NO_3^- yielded by this force field. The interface is defined by a ~1 nm region where water density gradually drops from its bulk value to zero. Indeed, HNO_3 accumulates at the interface, while NO_3^- ions remain largely excluded from this region. A simplified analysis, rooted in equilibrium thermodynamics, suggested a pK_a increase of up to one unit for HNO_3 at the interface, indicating that nitric acid becomes a weaker acid in this environment [36]. It should be noted, however, that this estimate assumes no local pH variation, implying a uniform H_3O^+ distribution. Theoretical studies suggest that water auto-ionization may be slightly enhanced near the interface [117], potentially increasing local H_3O^+ concentrations and reducing the magnitude of the estimated pK_a shift.

These results help reconcile divergent experimental findings on the interfacial stabilization of nitric acid in its protonated form. X-ray photoelectron spectroscopy (XPS) indicated a ~20% reduction in HNO_3 ionization at the solution interface [112]. This value may be an underestimate, as XPS cannot readily distinguish contributions from the topmost layer and subsurface regions. Indeed, MD simulations using the GROMOS-RONS force field suggest that HNO_3 enrichment is confined to a narrow, 1 nm-thick interfacial layer, below the spatial resolution of many experimental techniques. This explains why glancing-angle Raman spectroscopy, with a probing depth of 50−100 nm, detected no significant change in HNO_3 ionization [118].

Another intriguing spectroscopic observation is that the pairing between NO_2^- and its counterions strengthens at the water-air interface [119]. As already demonstrated in Fig. 7, ions like NO_3^- tend to be excluded from the interface, and this also applies to NO_2^-. However, Fig. 8 shows that, for the few NO_2^- ions that reach the surface, ion pairing is favored. Experimental techniques probing nitrogen oxyanions at the interface are thus likely to detect a signal with a larger contribution from ion pairs. Interfacial solution properties, such as surface tension, may also be influenced by the increased prevalence of ion pairs over dissociated ions at the surface.
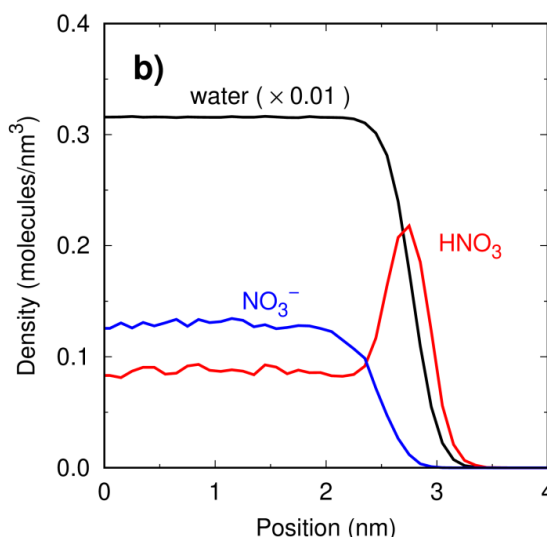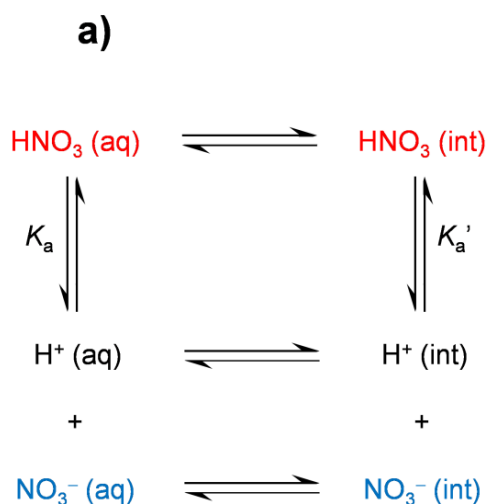
Fig. 7. (a) Thermodynamic cycle relating the local value of the ionization constant K_a of HNO_3 to the water/interface partition equilibria of the involved species. (b) Distribution of HNO_3 and NO_3^- at the water-air interface. Data replotted from ref. [36].
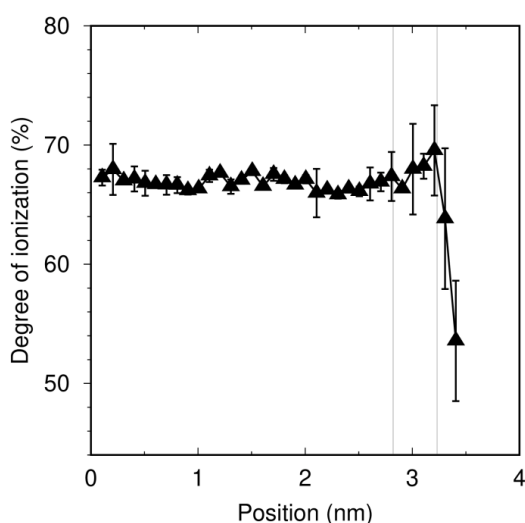
Fig. 8. Variations of the ion pairing tendency of $NaNO_2$ across the water-air interface. Vertical lines delimit the interface region where water density drops from 90 to 10 % of its bulk value. Data replotted from ref. [36].

The high surface-to-volume ratios of aqueous aerosol particles amplify the influence of the water-air interface on chemical speciation. While the GROMOS-RONS force field cannot explicitly model interconversion between nitrogen oxyanions and oxyacids, it successfully captured the preference for protonated forms and enhanced ion pairing at the interface. *Ab initio* MD simulations remain the gold standard for probing reaction dynamics, but their short time scales—constrained by computational limits—hinder broader exploration. In contrast, a classical model like GROMOS-RONS enables robust statistical analysis of molecular diffusion, partitioning, and reorientation over longer periods. Its reliable, validated parameters can generate realistic hydration and interaction configurations at the interface, providing ideal starting points for detailed *ab initio* studies of chemical reactions.

8. Where do we go from here?

This review chronicles a decade of developing and applying the GROMOS-RONS force field. Its robust, validated

parameters have illuminated experimental findings, offering insights into: *i*) how membrane environments modulate RONS concentration, availability, and reactivity; *ii*) redox signaling through protein-mediated RONS transport across membranes; and *iii*) acid-base equilibrium shifts and enhanced ion pairing at water-air interfaces. These applications highlight the force field's role as a bridge between simulation and experiment.

Looking forward, the GROMOS-RONS framework opens exciting avenues to explore new RONS species or apply existing models to novel systems. For instance, simulations could investigate RONS interactions with protein binding sites, such as those in superoxide dismutase, which regulates oxidative stress by scavenging RONS. Although classical, non-reactive MD cannot directly capture chemical reactions, the studies reviewed here demonstrate that RONS distributions, interactions, and dynamics yield critical indirect clues about local reactivity. Moreover, the long timescales accessible to MD enable investigation of larger systems. With computational advances, simulations of entire viral capsids have become feasible [120-122], offering the potential to track exogenously generated RONS in real time, in their way from the external environment, through the capsid barrier, down to the viral RNA. Simulations of such systems, which heavily rely on computational efficiency, could offer valuable insights for applications related to RONS-based therapies and disinfection. The versatility of GROMOS-RONS also extends to emerging fields like plasma medicine, where RONS drive therapeutic outcomes, and climate modeling, where aerosol chemistry shapes global processes. With openly accessible parameters and supporting files [33], the GROMOS-RONS force field invites researchers to adopt and extend it, fostering discoveries across diverse scientific domains.

Acknowledgments

Author Contributions

This text was written with support from artificial intelligence (Grok AI), with inputs and careful revision by the author. All figures were manually built by the author based on legitimate scientific data being reviewed.

References and Notes

[1] Commoner, B.; Townsend, J.; Pake, G. E. *Nature* **1954**, *174*, 689. **[Crossref]**

[2] Dröge, W. *Physiol. Rev.* **2002**, *82*, 47. **[Crossref]**

[3] Halliwell, B. *Encycl. Life Sci.* **2005**, 1. **[Crossref]**

[4] Halliwell, B.; Gutteridge, J. M. C. *Biochem. J.* **1984**, *219*, 1. **[Crossref]**

[5] Harman, D. *Proc. Natl. Acad. Sci. U. S. A.* **1981**, *78*, 7124. **[Crossref]**

[6] Radi, R. *Proc. Natl. Acad. Sci. U. S. A.* **2004**, *101*, 4003. **[Crossref]**

[7] Sanz, A.; Pamplona, R.; Barja, G. *Antioxid. Redox Signal.* **2006**, *8*, 582. **[Crossref]**

[8] Szabó, C.; Ischiropoulos, H.; Radi, R. *Nat. Rev. Drug Discovery* **2007**, *6*, 662. **[Crossref]**

[9] Ochsner, M. *J. Photochem. Photobiol. B* **1997**, *39*, 1. **[Crossref]**

[10] Laroussi, M. *Plasma* **2018**, *1*, 47. **[Crossref]**

[11] Brown, S. B.; Brown, E. A.; Walker, I. *Lancet Oncol.* **2004**, *5*, 497. **[Crossref]**

[12] Baptista, M. S.; Wainwright, M. *Braz. J. Med. Biol. Res.* **2011**, *44*, 1. **[Crossref]**

[13] Martins-Costa, M. T. C.; Anglada, J. M.; Francisco, J. S.; Ruiz-Lopez, M. F. *Angew. Chem., Int. Ed.* **2012**, *51*, 5413. **[Crossref]**

[14] Afri, M.; Gottlieb, H. E.; Frimer, A. A. *Free Radical Biol. Med.* **2002**, *32*, 605. **[Crossref]**

[15] Fortier, C. A.; Guan, B.; Cole, R. B.; Tarr, M. A. *Free Radical Biol. Med.* **2009**, *46*, 1376. **[Crossref]**

[16] Gamliel, A.; Afri, M.; Frimer, A. A. *Free Radical Biol. Med.* **2008**, *44*, 1394. **[Crossref]**

[17] Bartesaghi, S.; Valez, V.; Trujillo, M.; Peluffo, G.; Romero, N.; Zhang, H.; Kalyanaraman, B.; Radi, R. *Biochemistry* **2006**, *45*, 6813. **[Crossref]**

[18] Zhang, H.; Joseph, J.; Feix, J.; Hogg, N.; Kalyanaraman, B. *Biochemistry* **2001**, *40*, 7675. **[Crossref]**

[19] Zhang, H.; Bhargava, K.; Keszler, A.; Feix, J.; Hogg, N.; Joseph, J.; Kalyanaraman, B. *J. Biol. Chem.* **2003**, *278*, 8969. **[Crossref]**

[20] Kyrychenko, A.; Ladokhin, A. S. *J. Phys. Chem. B* **2013**, *117*, 5875. **[Crossref]**

[21] Xu, G.; Chance, M. R. *Chem. Rev.* **2007**, *107*, 3514. **[Crossref]**

[22] Charvátová, O.; Foley, B. L.; Bern, M. W.; Sharp, J. S.; Orlando, R.; Woods, R. J. *J. Am. Soc. Mass Spectrom.* **2008**, *19*, 1692. **[Crossref]**

[23] Pan, Y.; Stocks, B. B.; Brown, L.; Konermann, L. *Anal. Chem.* **2009**, *81*, 28. **[Crossref]**

[24] Pan, Y.; Ruan, X.; Valvano, M. A.; Konermann, L. *J. Am. Soc. Mass Spectrom.* **2012**, *23*, 889. **[Crossref]**

[25] Allen, M. P.; Tildesley, D. J. *Computer Simulation of Liquids*; Clarendon Press, 2009.

[26] Frenkel, D.; Smit, B. *Understanding Molecular Simulation: From Algorithms to Applications*; Academic Press, 2001.

[27] Chung, Y.-H.; Xia, J.; Margulis, C. J. *J. Phys. Chem. B* **2007**, *111*, 13336. **[Crossref]**

[28] Domínguez, L.; Sosa-Peinado, A.; Hansberg, W. *Arch. Biochem. Biophys.* **2010**, *500*, 82. **[Crossref]**

[29] Dynowski, M.; Schaaf, G.; Loque, D.; Moran, O.; Ludewig, U. *Biochem. J.* **2008**, *414*, 53. **[Crossref]**

[30] Cordeiro, R. M. *Biochim. Biophys. Acta, Biomembr.* **2014**, *1838*, 438. **[Crossref]**

[31] Cordeiro, R. M. *Biochim. Biophys. Acta* **2015**, *1850*, 1786. **[Crossref]**

[32] Sies, H. *Eur. J. Biochem.* **1993**, *215*, 213. **[Crossref]**

[33] Cordeiro, R. M. *J. Phys. Chem. B* **2025**, *129*, 5707. **[Crossref]**

[34] Cordeiro, R. M. *J. Phys. Chem. B* **2018**, *122*, 8211. **[Crossref]**

[35] Bacellar, I. O. L.; Cordeiro, R. M.; Mahling, P.; Baptista, M. S.; Röder, B.; Hackbarth, S. *Biochim. Biophys. Acta, Biomembr.* **2019**, *1861*, 879. **[Crossref]**

[36] Cordeiro, R. M.; Yusupov, M.; Razzokov, J.; Bogaerts, A. *J. Phys. Chem. B* **2020**, *124*, 1082. **[Crossref]**

[37] Razzokov, J.; Yusupov, M.; Cordeiro, R. M.; Bogaerts, A. *J. Phys. D: Appl. Phys.* **2018**, *51*, 365203. **[Crossref]**

[38] Oostenbrink, C.; Villa, A.; Mark, A. E.; Van Gunsteren, W. F. *J. Comput. Chem.* **2004**, *25*, 1656. **[Crossref]**

[39] Schmid, N.; Eichenberger, A. P.; Choutko, A.; Riniker, S.; Winger, M.; Mark, A. E.; van Gunsteren, W. F. *Eur. Biophys. J.* **2011**, *40*, 843. **[Crossref]**

[40] Sander, R. *Atmos. Chem. Phys.* **2023**, *23*, 10901. **[Crossref]**

[41] Poger, D.; Mark, A. E. *J. Chem. Theory Comput.* **2010**, *6*, 325. **[Crossref]**

[42] Poger, D.; van Gunsteren, W. F.; Mark, A. E. *J. Comput. Chem.* **2010**, *31*, 1117. **[Crossref]**

[43] Petrov, D.; Margreitter, C.; Grandits, M.; Oostenbrink, C.; Zagrovic, B. *PLoS Comput. Biol.* **2013**, *9*, e1003154. **[Crossref]**

[44] Koppenol, W. H.; Bounds, P. L.; Nauser, T.; Kissner, R.; Rüegger, H. *Dalton Trans.* **2012**, *41*, 13779. **[Crossref]**

[45] Wild, J. D.; Sridhar, T.; Potter, O. E. *Chem. Eng. J.* **1978**, *15*, 209. **[Crossref]**

[46] Battino, R.; Rettich, T. R.; Tominaga, T. *J. Phys. Chem. Ref. Data* **1983**, *12*, 163. **[Crossref]**

[47] Biń, A. K. *Ozone: Sci. Eng.* **2006**, *28*, 67. **[Crossref]**

[48] Lur'e, B. A.; Arkhipov, I. V.; Apal'kova, V. N. *Russ. J. Phys. Chem.* **1986**, *60*, 1144.

[49] Squadrito, G. L.; Postlethwait, E. M. *Nitric Oxide* **2009**, *21*, 104. **[Crossref]**

[50] Young, C. L., Ed. *Oxides of Nitrogen, IUPAC Solubility Data Series*; Pergamon Press: Oxford, England, 1981; Vol. 8.

[51] Riddell, J. D.; Lockwood, D. J.; Irish, D. E. *Can. J. Chem.* **1972**, *50*, 2951. **[Crossref]**

[52] Liu, X.; Miller, M. J.; Joshi, M. S.; Thomas, D. D.; Lancaster, J. R., Jr. *Proc. Natl. Acad. Sci. USA* **1998**, *95*, 2175. **[Crossref]**

[53] Marrink, S.-J.; Berendsen, H. J. C. *J. Phys. Chem.* **1994**, *98*, 4155. **[Crossref]**

[54] Möller, M. N.; Li, Q.; Chinnaraj, M.; Cheung, H. C.; Lancaster, J. R.; Denicola, A. *Biochim. Biophys. Acta Biomembr.* **2016**, *1858*, 2923. **[Crossref]**

[55] Subczynski, W. K.; Hyde, J. S. *Biophys. J.* **1983**, *41*, 283. **[Crossref]**

[56] Norlén, L. *J. Investig. Dermatol.* **2001**, *117*, 830. **[Crossref]**

[57] Lingwood, D.; Simons, K. *Science* **2010**, *327*, 46. **[Crossref]**

[58] Aresta-Branco, F.; Cordeiro, A. M.; Marinho, H. S.; Cyrne, L.; Antunes, F.; de Almeida, R. F. M. *J. Biol. Chem.* **2011**, *286*, 5043. **[Crossref]**

[59] Vecer, J.; Vesela, P.; Malinsky, J.; Herman, P. *FEBS Lett.* **2014**, *588*, 443. **[Crossref]**

[60] Engelmann, F. M.; Mayer, I.; Gabrielli, D. S.; Toma, H. E.; Kowaltowski, A. J.; Araki, K.; Baptista, M. S. *J. Bioenerg. Biomembr.* **2007**, *39*, 175. **[Crossref]**

[61] Cordeiro, R. M.; Miotto, R.; Baptista, M. S. *J. Phys. Chem. B* **2012**, *116*, 14618. **[Crossref]**

[62] Miotto, R.; Costa, E. B.; Trellese, G. G.; Neto, A. J. P.; Baptista, M. S.; Ferraz, A. C.; Cordeiro, R. M. in *Emerging Trends in Applications and Infrastructures for Computational Biology, Bioinformatics, and Systems Biology: Systems and Applications*; Tran, Q. N., Arabnia, H. R., Eds.; Elsevier, 2016; pp 197-211.

[63] Möller, M. N.; Lancaster, J. R., Jr.; Denicola, A. in *Current Topics in Membranes*; Matalon, S., Ed.; Elsevier, 2008; pp 23–42.

[64] de Grey, A. D. N. J. *DNA Cell Biol.* **2002**, *21*, 251. **[Crossref]**

[65] Bielski, B. H. J.; Arudi, R. L.; Sutherland, M. W. *J. Biol. Chem.* **1983**, *258*, 4759. **[Crossref]**

[66] Gebicki, J. M.; Bielski, B. H. J. *J. Am. Chem. Soc.* **1981**, *103*, 7020. **[Crossref]**

[67] Fukuzawa, K.; Gebicki, J. M. *Arch. Biochem. Biophys.* **1983**, *226*, 242. **[Crossref]**

[68] Gus'kova, R. A.; Ivanov, I. I.; Kol'tover, V. K.; Akhobadze, V. V.; Rubin, A. B. *Biochim. Biophys. Acta* **1984**, *778*, 579. **[Crossref]**

[69] Yusupov, M.; Van der Paal, J.; Neyts, E. C.; Bogaerts, A. *Biochim. Biophys. Acta* **2017**, *1861*, 839. **[Crossref]**

[70] van der Paal, J.; Verheyen, C.; Neyts, E. C.; Bogaerts, A. *Sci. Rep.* **2017**, *7*, 39526. **[Crossref]**

[71] Beckman, J. S.; Koppenol, W. H. *Am. J. Physiol. Cell Physiol.* **1996**, *271*, C1424. **[Crossref]**

[72] Cheng, Z.; Li, Y. *Chem. Rev.* **2007**, *107*, 748. **[Crossref]**

[73] Prousek, J. *Pure Appl. Chem.* **2007**, *79*, 2325. **[Crossref]**

[74] Augusto, O.; Miyamoto, S. in *Principles of Free Radical Medicine, Volume 1*; Pantopoulos, K., Schipper, H. M., Eds.; Nova Science, 2011.

[75] Ferrer-Sueta, G.; Radi, R. *ACS Chem. Biol.* **2009**, *4*, 161. **[Crossref]**

[76] Denicola, A.; Souza, J. M.; Radi, R. *Proc. Natl. Acad. Sci. USA* **1998**, *95*, 3566. **[Crossref]**

[77] McGrath, M. P.; Rowland, F. S. *J. Phys. Chem.* **1994**, *98*, 1061. **[Crossref]**

[78] McGrath, M. P.; Rowland, F. S. *J. Chem. Phys.* **2005**, *122*, 134312. **[Crossref]**

[79] Berski, S.; Latajka, Z.; Gordon, A. J. *J. Comput. Chem.* **2011**, *32*, 1528. **[Crossref]**

[80] Agre, P.; Bonhivers, M.; Borgnia, M. J. *J. Biol. Chem.* **1998**, *273*, 14659. **[Crossref]**

[81] Agre, P. *Angew. Chem., Int. Ed.* **2004**, *43*, 4278. **[Crossref]**

[82] Murata, K.; Mitsuoka, K.; Hirai, T.; Walz, T.; Agre, P.; Heymann, J. B.; Engel, A.; Fujiyoshi, Y. *Nature* **2000**, *407*, 599. **[Crossref]**

[83] Sui, H.; Han, B.-G.; Lee, J. K.; Walian, P.; Jap, B. K. *Nature* **2001**, *414*, 872. **[Crossref]**

[84] Törnroth-Horsefield, S.; Wang, Y.; Hedfalk, K.; Johanson, U.; Karlsson, M.; Tajkhorshid, E.; Neutze, R.; Kjellbom, P. *Nature* **2006**, *439*, 688. **[Crossref]**

[85] Tajkhorshid, E.; Nollert, P.; Jensen, M. Ø.; Miercke, L. J. W.; O'Connell, J.; Stroud, R. M.; Schulten, K. *Science* **2002**, *296*, 525. **[Crossref]**

[86] Smolin, N.; Li, B.; Beck, D. A. C.; Daggett, V. *Biophys. J.* **2008**, *95*, 1089. **[Crossref]**

[87] Wang, Y.; Tajkhorshid, E. *J. Nutr.* **2007**, *137*, 1509S. **[Crossref]**

[88] Wang, Y.; Shaikh, S. A.; Tajkhorshid, E. *Physiology* **2010**, *25*, 142. **[Crossref]**

[89] de Groot, B. L.; Grubmüller, H. *Science* **2001**, *294*, 2353. [Crossref]

[90] de Groot, B. L.; Frigato, T.; Helms, V.; Grubmüller, H. *J. Mol. Biol.* **2003**, *333*, 279. [Crossref]

[91] de Groot, B. L.; Grubmüller, H. *Curr. Opin. Struct. Biol.* **2005**, *15*, 176. [Crossref]

[92] Jensen, M. Ø.; Tajkhorshid, E.; Schulten, K. *Biophys. J.* **2003**, *85*, 2884. [Crossref]

[93] Jensen, M. Ø.; Röthlisberger, U.; Rovira, C. *Biophys. J.* **2005**, *89*, 1744. [Crossref]

[94] Bienert, G. P.; Schjoerring, J. K.; Jahn, T. P. *Biochim. Biophys. Acta, Biomembr.* **2006**, *1758*, 994. [Crossref]

[95] Bienert, G. P.; Møller, A. L. B.; Kristiansen, K. A.; Schulz, A.; Møller, I. M.; Schjoerring, J. K.; Jahn, T. P. *J. Biol. Chem.* **2007**, *282*, 1183. [Crossref]

[96] Bienert, G. P.; Chaumont, F. *Biochim. Biophys. Acta* **2014**, *1840*, 1596. [Crossref]

[97] Ye, Q.; Steudle, E. *Plant Cell Environ.* **2006**, *29*, 459. [Crossref]

[98] Kim, Y. X.; Steudle, E. *J. Exp. Bot.* **2009**, *60*, 547. [Crossref]

[99] Henzler, T.; Ye, Q.; Steudle, E. *Plant Cell Environ.* **2004**, *27*, 1184. [Crossref]

[100] Almasalmeh, A.; Krenc, D.; Wu, B.; Beitz, E. *FEBS J.* **2014**, *281*, 647. [Crossref]

[101] Orrico, F.; Lopez, A. C.; Saliwonczyk, D.; Acosta, C.; Rodriguez-Grecco, I.; Mouro-Chanteloup, I.; Ostuni, M. A.; Denicola, A.; Thomson, L.; Möller, M. N. *J. Biol. Chem.* **2022**, *298*, 101503. [Crossref]

[102] Orrico, F.; Lopez, A. C.; Silva, N.; Franco, M.; Mouro-Chanteloup, I.; Denicola, A.; Ostuni, M. A.; Thomson, L.; Möller, M. N. *Free Radic. Biol. Med.* **2025**, *230*, 389. [Crossref]

[103] Yusupov, M.; Razzokov, J.; Cordeiro, R. M.; Bogaerts, A. *Oxid. Med. Cell. Longev.* **2019**, *2019*, 2930504. [Crossref]

[104] Cui, Y.; Zhao, T.; Wang, Z.; Wang, X.; Wang, D.; Zhang, Y. *Phys. Plasmas* **2023**, *30*, 063509. [Crossref]

[105] Hu, X.; Jin, X.; Xing, R.; Liu, Y.; Feng, Y.; Lyu, Y.; Zhang, R. *Results Phys.* **2023**, *50*, 106621. [Crossref]

[106] Yan, D.; Talbot, A.; Nourmohammadi, N.; Sherman, J. H.; Cheng, X.; Keidar, M. *Biointerphases* **2015**, *10*, 040801. [Crossref]

[107] Pan, Y.; Piyadasa, H.; O'Neil, J. D.; Konermann, L. *J. Mol. Biol.* **2012**, *416*, 400. [Crossref]

[108] Konermann, L.; Pan, Y. *Expert Rev. Proteomics* **2012**, *9*, 497. [Crossref]

[109] Roeselová, M.; Vieceli, J.; Dang, L. X.; Garrett, B. C.; Tobias, D. J. *J. Am. Chem. Soc.* **2004**, *126*, 16308. [Crossref]

[110] Vácha, R.; Slavíček, P.; Mucha, M.; Finlayson-Pitts, B. J.; Jungwirth, P. *J. Phys. Chem. A* **2004**, *108*, 11573. [Crossref]

[111] Vieceli, J.; Roeselová, M.; Potter, N.; Dang, L. X.; Garrett, B. C.; Tobias, D. J. *J. Phys. Chem. B* **2005**, *109*, 15876. [Crossref]

[112] Lewis, T.; Winter, B.; Stern, A. C.; Baer, M. D.; Mundy, C. J.; Tobias, D. J.; Hemminger, J. C. *J. Phys. Chem. C* **2011**, *115*, 21183. [Crossref]

[113] Shamay, E. S.; Buch, V.; Parrinello, M.; Richmond, G. L. *J. Am. Chem. Soc.* **2007**, *129*, 12910. [Crossref]

[114] Ardura, D.; Donaldson, D. J. *Phys. Chem. Chem. Phys.* **2009**, *11*, 857. [Crossref]

[115] Wang, S.; Bianco, R.; Hynes, J. T. *J. Phys. Chem. A* **2009**, *113*, 1295. [Crossref]

[116] Baer, M. D.; Tobias, D. J.; Mundy, C. J. *J. Phys. Chem. C* **2014**, *118*, 29412. [Crossref]

[117] Hub, J. S.; Wolf, M. G.; Caleman, C.; van Maaren, P. J.; Groenhof, G.; van der Spoel, D. *Chem. Sci.* **2014**, *5*, 1745. [Crossref]

[118] Wren, S. N.; Donaldson, D. J. *Chem. Phys. Lett.* **2012**, *522*, 1. [Crossref]

[119] Otten, D. E.; Onorato, R.; Michaels, R.; Goodknight, J.; Saykally, R. J. *Chem. Phys. Lett.* **2012**, *519−520*, 45. [Crossref]

[120] Freddolino, P. L.; Arkhipov, A. S.; Larson, S. B.; McPherson, A.; Schulten, K. *Structure* **2006**, *14*, 437. [Crossref]

[121] Larsson, D. S. D.; Liljas, L.; van der Spoel, D. *PLoS Comput. Biol.* **2012**, *8*, e1002502. [Crossref]

[122] Tarasova, E.; Nerukh, D. *J. Phys. Chem. Lett.* **2018**, *9*, 5805. [Crossref]

How to cite this article